ISBN: 978-3-95450-247-9 ISSN: 2673-5490 doi: 10.18429/JACoW-IPAC2024-THPS56

FIELD CHARACTERIZATION OF AXIALLY AND RADIALLY MAGNETIZED NEODYMIUM RINGS

T. Xu*, S. D. Anderson, R. J. England
SLAC National Accelerator Laboratory, Menlo Park, CA, USA

Abstract

Permanent magnets are attractive options for nano focusing and q-magnification in MeV ultrafast electron diffraction (MeV-UED) due to their high field strengths and compact footprints. In this work, we present field characterization of axially and radially magnetized neodymium rings. Such rings can produce strong axisymmetric focusing and naturally fulfill the requirement of stigmatic imaging for post-sample optical systems. Field qualities of the rings and their application in MeV-UED are studied and presented.

INTRODUCTION

Magnetic lenses are crucial components of keV electron microsopy and diffraction instruments and enable magnification of small sample features spanning from a few times to over a million times. For relativistic electrons with energies in the MeV range, the challenge for developing a strong lens lies in the decreasing focusing strength of the solenoidal lens since the focal lengths scale as γ^{-2}. An approach to achieve shorter focal length consists in using permanent magnetic quadrupoles (PMQ) as the focal length of quadrupole only decreases as γ^{-1} and PMQs can reach very high field gradients [1, 2]. However, it would require at least three PMQs to achieve stigmatic imaging condition (equal magnification in x and y) and the longitudinal distances between them need to be precisely adjusted. Coupled with manufacturing and alignment errors, it makes PMQs difficult to tune during operation.

Permanent magnetic solenoid (PMS) is an interesting alternative to PMQ for focusing MeV electron beams [3–5]. Similar to PMQs, PMSs are based on rare earth alloys like samarium cobalt or Neodymium (NdFeB) magnet but the orientation of the magnetization is configured in a way to produce solenoidal fields. There're two types of configurations: axially and radially magnetized PMS; see Fig. 1. For simplicity we will refer them as axial PMS and radial PMS. While the scaling of focal strength of a PMS still follows γ^{-2}, the large remanence of PMS supports a strong axial field and produces a short focal length, e.g., a few centimeters at a few MeVs. Furthermore, the focusing provided by a PMS is axisymmetric and one could achieve stigmatic imaging by adjusting the position of a single magnet.

Several neodymium PMS rings are being developed at the SLAC MeV-UED facility for nano focusing and angular magnification. In this paper, we report the field characterization of the axial and radial PMS rings. Field qualities of the PMS rings are evaluated with magnetization and Hall probe measurements. Based on the measurements, different simulation models are used to estimate their focusing strengths and the effects of manufacturing flaws. Beam dynamics simulation shows a PMS lens pair (objective lens and eyepiece) can produce over five times magnification for MeV-UED.

* txu@slac.stanford.edu

h

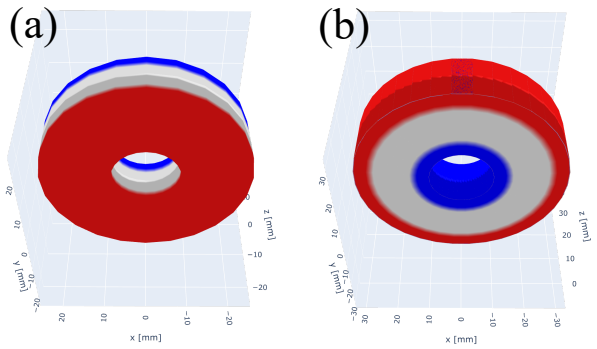

Figure 1: Mockups of (a) an axially magnetized PMS and (b) a radially magnetizede PMS. The red and blue color denote north and south poles of the magnets.

AXIAL PMS

The on-axis magnetic field of an axial PMS can be calculated using a surface current model [6] and follows as,

$$B_{z,\mathrm{pms,a}} = B_{z,\mathrm{sol}}(z, R_i, L) - B_{z,\mathrm{sol}}(z, R_o, L) \qquad (1)$$

where $B_{z,\mathrm{sol}}$ is the on-axis field of a solenoid of zero thickness and is given by,

$$B_{z,\mathrm{sol}}(z, R, L) = \frac{B_r}{2}\left(\frac{z + L/2}{\sqrt{(z + L/2)^2 + R^2}} - \frac{z - L/2}{\sqrt{(z - L/2)^2 + R^2}}\right) \qquad (2)$$

here L, R_i, R_o are length, inner and outer radii of the PMS ring, and B_r is the remanence.

To achieve high on-axis field and short focal length, a smaller inner radius R_i is required for axial PMS. We have purchased a batch of four axial PMS rings with R_i=2.38mm, R_o=25.4mm, L=12.7mm. The PMSs are made of grade N42 NdFeB and have an nominal remanence of 1.32T. For electron beams with 4.2 MeV kinetic energy, the focal length is estimated to be 10.8 cm.

We measured the on-axis fields of the axial PMSs with a 1D Hall probe and the results are shown in Fig. 2. The

ISBN: 978-3-95450-247-9 ISSN: 2673-5490 doi: 10.18429/JACoW-IPAC2024-THPS56

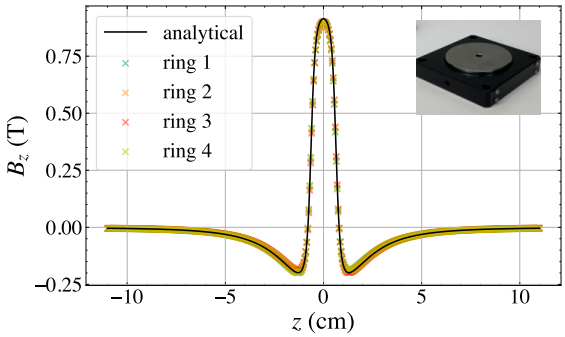

Figure 2: Analytical and measured on-axis fields of axial PMSs. The inset shows a photo of a measured PMS.

Table 1: Measured magnetization of the four axial PMSs and the corresponding kicks calculated with RADIA.

	Magnetization (mT)			kick (mrad)	
Ring #	$\mu_0 M_x$	$\mu_0 M_y$	$\mu_0 M_z$	$\Delta x'$	$\Delta y'$
1	7.98	0.51	1318.2	0	0.21
2	3.14	-1.1	1315.8	0.03	0.08
3	-7.91	11.52	1318.6	-0.32	-0.19
4	4.6	8.12	1318.9	-0.20	0.13

measured profiles agree well with the analytical form (Eq. 1) when B_r is set to be 1.318T.

To evaluate the impact of flawed magnetization on beam dynamics, we measured the magnetizations of the PMS and use a RADIA model to compute the trajectories of a 4.2 MeV electron when it travels through each PMS. In real magnets, the small tilt angle between the magnetization and magnet axis results in a kick in both x and y. The measured magnetization along with the kick calculated by RADIA are listed in Table 1. The kicks are found to small and correctable by steering magnets.

RADIAL PMS

The on-axis magnetic field of a radial PMS is given by

$$B_{z,\mathrm{pms,r}} = B_{z,\mathrm{disk}}(z + L/2) - B_{z,\mathrm{disk}}(z - L/2) \quad (3)$$

where $B_{z,\mathrm{disk}}$ is the on-axis field of a thin current disk,

$$B_{z,\,\mathrm{disk}}\,(z) = \frac{B_r}{2}\left(\ln\frac{\sqrt{z^2+R_o^2}+R_o}{\sqrt{z^2+R_i^2}+R_i} - \frac{R_o}{\sqrt{z^2+R_o^2}} + \frac{R_i}{\sqrt{z^2+R_i^2}}\right) \quad (4)$$

Compared with axial PMSs, radial PMSs have weaker stray fields and one can combine a pair of radial PMSs with opposite magnetization (inward and outward) to enhance the on-axis field.

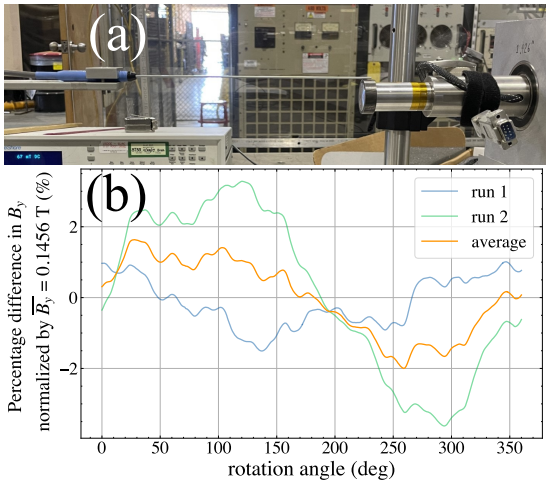

Figure 3: (a) Setup and (b) results of the rotation measurement for hot-pressed radial PMS.

Hot-Pressed Radial PMS

A radial PMS can be produced with the hot-press method [7]. To assess the performance and field quality of the hot-pressed radial PMS, we have ordered several sample radial PMSs from a magnet vendor and performed rotation measurements to characterize the azimuthal uniformity of magnetization. The setup of the rotation measurement is shown in Fig. 3(a). A 1D Hall probe was placed above the PMS to measure the vertical magnetic field component while the ring was rotated by a motor. To eliminate the effect of the runout, two measurements were made for each ring, with the holding mechanism turned 180 degrees between the first and second measurement. The runout effect is minimized if one averages two sets of data. The measured fields of a sample ring is depicted in Fig. 3(b) and shows that the peak-to-peak fluctuation of the field is within 2%.

Upon further communication with the magnet vendor, we found the dimensions of hot-press rings were limited—the ratio of the inner and outer radii of the ring needs to greater than 0.8. In addition, the length of the ring is recommended to be about half the of the inner radius. To achieve our desired dimensions, the ring would have to be segmented both radially and longitudinally. The assembly of these rings would be challenging due to the repelling forces between each longitudinal pieces. While this makes hot-pressed radial PMS infeasible for our design, the method still remains an attractive solution to make one-piece radial PMSs for other uses.

Wedge-Based Radial PMS

Due to the difficulty to produce a radial PMS with the hot-press technique for our desired dimensions, we adopt a more conventional method and segment the ring azimuthally into eight identical wedges, with each wedge diametrically magnetized inward or outward. To characterize the field performance of the wedge-based radial PMS, we performed

ISBN: 978-3-95450-247-9 ISSN: 2673-5490 doi: 10.18429/JACoW-IPAC2024-THPS56

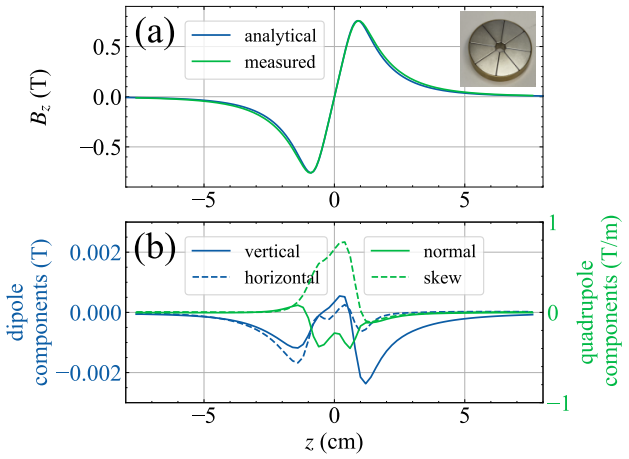

Figure 4: On-axis field measurement (a) and generalized gradients (b) of the wedge-based PMS (shown in the inset).

a Hall probe scan and the 3D field map obtained was used to calculate the generalized gradients and transfer maps of the magnet [8, 9]. The measured on-axis field as well as the dipole and quadrupole components of the generalized gradients are shown in Fig. 4. Based on the the measured field, we performed ELEGANT simulation and found a focal length of 7.8 cm and a kick of $\Delta x'$=4 mrad and $\Delta y'$=1 mrad is expected for a 4.2 MeV beam. To minimize the kick, a proper arrangement of the dual ring setup is required by pairing two PMSs with opposite dipole field polarities.

APPLICATION IN MEV-UED

The strong field strength of PMSs makes them attractive options for post-sample magnetic optics to enhance reciprocal space resolution in MeV-UED [10]. In an MeV-UED beamline, electrons are scattered by a sample and the scattering angles x_i' are converted into spatial offsets x_f on the detector by a drift l_d,

$$x_f = x_0 + l_d x_i' \approx l_d x_i' \tag{5}$$

Adding magnetic optics downstream of the sample allows the effective camera length (transfer matrix element R_{12}) to be varied. As illustrated in Fig. 5(b), an objective lens of focal length f_{obj} maps the scattering angles x_i' into spatial offsets at its back focal plane (BFP). The virtual image is then magnified by an eyepiece lens of focal length f_{eye} over distance l_e . For a strong eyepiece lens ($f_{\mathrm{eye}} \ll l_e$), x_f and x_i' are related by,

$$x_f \approx \frac{f_{\mathrm{obj}} l_e}{f_{\mathrm{eye}}} x_i' \tag{6}$$

With proper choice of of f_{obj} and f_{eye}, the camera length can be made larger than l_d which allows angular magnification of the diffraction.

Here we consider an angular magnification setup at SLAC MeV-UED facility and use two axial PMSs as objective lens and eyepiece. The dimensions and focal length of the two PMSs are listed in Table 2. For a total drift distance

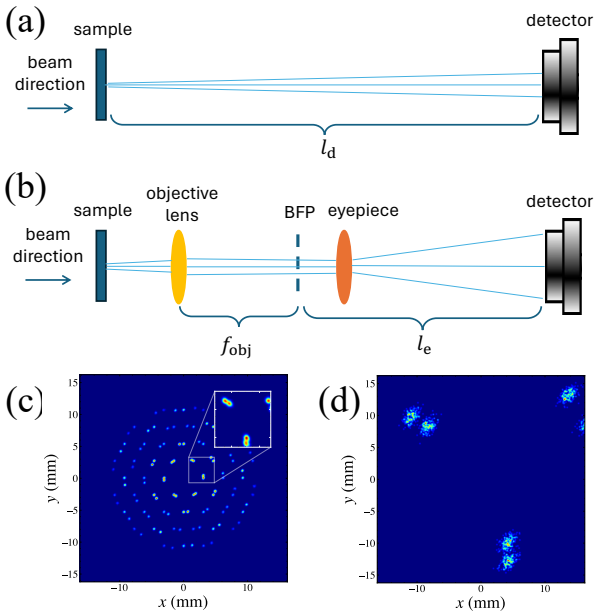

Figure 5: Cartoons of an electron diffraction beamline layout without angular magnification (a) and with angular magnification(b). (c) and (d) are the corresponding simulated diffraction pattern on detector. The inset in (c) shows the region of interest when zoomed in.

Table 2: Dimensions and focal lengths of the objective lens and eyepiece PMS.

	R_i (mm)	R_o (mm)	L(mm)	f (cm)
objective lens	3.175	9.525	6.35	67
eyepiece	3.175	38.1	25.4	6.23

l_d=3.63m, we estimate from Eq. 6 that a magnification of 8.5 can be achieved if the objective lens is positioned 10 cm downstream of sample. Start-to-end simulations were conducted using GPT for a bilayer WS_2 sample with 7 deg tilt. The diffraction patterns on the detector are shown in Fig. 5(c) for the case of no magnification and Fig. 5(d) when PMSs are present. It is clear that the diffraction pattern are magnified. We note that only a few of diffraction peaks can be captured due to limited detector size. In practice, one can use a steering magnet to direct different portions of the diffraction pattern through PMS and magnify the region of interest in reciprocal space.

CONCLUSION

In conclusion, we have presented the field characterization of axially and radially magnetized neodymium ring magnets. We show in simulation that angular magnification can be achieved with two PMSs as objective lens and eyepiece and a magnification of 8.5 can be achieved compared with drift. For future work we will install the PMSs in an accelerator beamline and test their performance for focusing and magnification.

ISBN: 978-3-95450-247-9 ISSN: 2673-5490 doi: 10.18429/JACoW-IPAC2024-THPS56

REFERENCES

[1] J. K. Lim, P. Frigola, G. Travish, J. B. Rosenzweig, S. G. Anderson, W. J. Brown, J. S. Jacob, C. L. Robbins, and A. M. Tremaine, "Adjustable, short focal length permanent-magnet quadrupole based electron beam final focus system," *Phys. Rev. ST Accel. Beams*, vol. 8, p. 072401, July 2005.

[2] D. Cesar, J. Maxson, P. Musumeci, Y. Sun, J. Harrison, P. Frigola, F. O'Shea, H. To, D. Alesini, and R. Li, "Demonstration of Single-Shot Picosecond Time-Resolved MeV Electron Imaging Using a Compact Permanent Magnet Quadrupole Based Lens," *Phys. Rev. Lett.*, vol. 117, p. 024801, July 2016.

[3] T. Gehrke, "Design of permanent magnetic solenoids for REGAE," Master's thesis, 2013.

[4] M. Hachmann, K. Flöttmann, T. Gehrke, and F. Mayet, "Design and characterization of permanent magnetic solenoids for REGAE," *Nucl. Instrum. Methods Phys. Res., Sect. A*, vol. 829, pp. 270–273, Sept. 2016.

[5] T. Burris-Mog, M. Burns, A. Chavez, and J. Schillig, "Analysis of an adjustable field permanent magnet solenoid," *Nucl. Instrum. Methods Phys. Res., Sect. A*, vol. 868, pp. 66–72, Oct. 2017.

[6] Q. Peng, S. McMurry, and J. Coey, "Axial magnetic field produced by axially and radially magnetized permanent rings," *Journal of Magnetism and Magnetic Materials*, vol. 268, pp. 165–169, Jan. 2004.

[7] W. Grünberger, D. Hinz, A. Kirchner, K.-H. Müller, and L. Schultz, "Hot deformation of nanocrystalline nd-fe-b alloys," *Journal of Alloys and Compounds*, vol. 257, no. 1-2, pp. 293–301, 1997.

[8] M. Venturini and A. J. Dragt, "Accurate computation of transfer maps from magnetic field data," *Nucl. Instrum. Methods Phys. Res., Sect. A*, vol. 437, pp. 387–392, 1999.

[9] M. Borland, "Elegant: A flexible sdds-compliant code for accelerator simulation," tech. rep., Argonne National Lab., IL (US), 2000.

[10] P. Denham, Y. Yang, V. Guo, A. Fisher, X. Shen, T. Xu, R. J. England, R. K. Li, and P. Musumeci, "High energy electron diffraction instrument with tunable camera length," *Structural Dynamics*, vol. 11, p. 024302, Mar. 2024.